

A dunite fragment in meteorite Northwest Africa (NWA) 11421: A piece of the Moon's mantle

ALLAN H. TREIMAN^{1,*} AND JULIA SEMPRICH^{2,†}

¹Lunar and Planetary Institute, 3600 Bay Area Boulevard, Houston, Texas 77058, U.S.A.

²AstrobiologyOU, School of Environment, Earth and Ecosystem Sciences, The Open University, Walton Hall, Milton Keynes MK7 6AA, U.K.

ABSTRACT

A centimeter-sized fragment of dunite, the first recognized fragment of Moon mantle material, has been discovered in the lunar highlands breccia meteorite Northwest Africa (NWA) 11421. The dunite consists of 95% olivine (Fo₈₃), with low-Ca and high-Ca pyroxenes, plagioclase, and chrome spinel. Mineral compositions vary little across the clast and are consistent with chemical equilibration. Mineral thermobarometry implies that the dunite equilibrated at 980 ± 20 °C and 0.4 ± 0.1 gigapascal (GPa) pressure. The pressure at the base of the Moon's crust (density 2550 kg/m³) is 0.14–0.18 GPa, so the dunite equilibrated well into the Moon's upper mantle. Assuming a mantle density of 3400 kg/m³, the dunite equilibrated at a depth of 88 ± 22 km. Its temperature and depth of equilibration are consistent with the calculated present-day selenotherm (i.e., lunar geotherm).

The dunite's composition, calculated from mineral analyses and proportions, contains less Al, Ti, etc., than chondritic material, implying that it is of a differentiated mantle (including cumulates from a lunar magma ocean). The absence of phases containing P, Zr, etc., suggests minimal involvement of a KREEP component, and the low proportion of Ti suggests minimal interaction with late melt fractionates from a lunar magma ocean. The Mg/Fe ratio of the dunite (Fo₈₃) is significantly lower than models of an overturned unmixed mantle would suggest, but is consistent with estimates of the bulk composition of the Moon's mantle.

Keywords: Moon, mantle, dunite, meteorite, thermobarometry, NWA 11421, selenotherm

INTRODUCTION

The Moon's mantle forms the greatest portion (by volume and mass) of the Moon, and figures prominently in all models of the Moon's origin and evolution (Shearer and Papike 1999; Elkins-Tanton et al. 2002b; Wicczorek et al. 2006, 2013). Until now, understanding of the lunar mantle has been hindered by the absence of samples of mantle material. Lacking lunar mantle material to examine, the composition and physical state of the Moon's mantle have been inferred from geophysical data and physico-chemical models: Apollo-era seismology (Kuskov and Kronrod 2009; Zhao et al. 2012; Matsumoto et al. 2015; Garcia et al. 2019); GRAIL measurements of gravity (Wicczorek et al. 2006; Matsuyama et al. 2016); and theoretical models based on those constraints and estimates of the Moon's bulk composition (Elkins-Tanton et al. 2002a; Wicczorek et al. 2006; Elkins-Tanton et al. 2011). Here, we present the first undisputable sample of the lunar mantle, and its implications for its origin.

Lunar evolution: Background

The standing model of the evolution of the lunar mantle starts as a planet-encompassing lunar magma ocean (LMO), produced during a collision between the proto-Earth and a planetesimal (e.g., Wicczorek et al. 2006; Elkins-Tanton et al. 2011). As the LMO cooled, it crystallized mafic minerals, olivine followed by low-Ca pyroxene and then augite, which sank to form cumulate

igneous rocks at the base of the ocean. The minerals became more ferroan (less magnesian) as crystallization proceeded. The mafic minerals accumulated in a chemically and mineralogically layered pile. Plagioclase was among the last minerals to crystallize, and it floated on the remaining LMO to form an anorthositic crust (Wood et al. 1970; Elkins-Tanton et al. 2011; Wicczorek et al. 2013). The last dregs of the LMO were rich in incompatible elements, titanium, and iron (the KREEP component), and were denser than the underlying mafic cumulates (Srivastava et al. 2022). The whole mantle was gravitationally unstable, with denser, ferroan material overlying lighter, magnesian material. Under the influence of gravity, the mantle overturned, bringing magnesian cumulates toward the surface and ferroan and Ti-rich materials to depth (Hess and Parmentier 1995; Elkins-Tanton et al. 2011). The overturned mantle could have been chemically layered, with the original stratigraphy essentially intact but inverted (Elkins-Tanton et al. 2011). Alternatively, the overturned mantle could have been mixed to various degrees (Boukaré et al. 2018; Zhao et al. 2019; Moriarty et al. 2021a; Schwinger and Breuer 2022). For a detailed summary see Gross and Joy (2016).

The lunar crust, originally the plagioclase flotation cumulates, is less than 45 km thick as calculated from gravity and seismic data (Wicczorek et al. 2013). It is reasonable that larger impact basins would have penetrated the crust and exposed and/or excavated lunar mantle material (Morrison 1998; Potter et al. 2012; Vaughan et al. 2013; Miljković et al. 2015; Moriarty et al. 2021a). Many outcrops of olivine rich material have been identified around lunar basins, and could represent uplifted mantle material (Nakamura et al. 2009; Yamamoto et

* E-mail: Treiman@lpi.usra.edu. Orcid 0000-0002-8073-2839

† Orcid 0000-0003-4398-0961


 Open access: Article available to all readers online.

TABLE 1. Average mineral compositions and calculated bulk composition for the D1 dunite

Analyses	Olivine 29		OPX 15		Augite 18		Chromite 3		Plagioclase 3		Dunite bulk Calculated	
SiO ₂	39.86	± 0.22	55.17	± 0.67	52.16	± 0.52	0.56	± 0.56	44.02	± 0.49	39.65	± 0.23
TiO ₂	0.04	± 0.01	0.58	± 0.06	1.14	± 0.22	1.61	± 0.25	0.01	± 0.01	0.07	± 0.01
Al ₂ O ₃	0.06	± 0.12	1.51	± 0.23	2.20	± 0.50	11.20	± 1.28	35.90	± 0.43	0.53	± 0.14
Cr ₂ O ₃	0.04	± 0.02	0.60	± 0.04	0.82	± 0.09	50.96	± 3.45	0.00	± 0.00	0.51	± 0.05
FeO	16.05	± 0.15	10.08	± 0.36	4.40	± 0.24	26.49	± 0.92	0.69	± 0.07	15.72	± 0.16
MnO	0.19	± 0.01	0.20	± 0.01	0.12	± 0.01	0.41	± 0.01	0.01	± 0.01	0.18	± 0.01
MgO	44.54	± 0.61	30.74	± 0.39	17.06	± 0.40	5.46	± 0.73	0.11	± 0.02	43.08	± 0.60
CaO	0.09	± 0.22	1.41	± 0.16	21.69	± 0.55	0.38	± 0.23	19.20	± 0.03	0.48	± 0.22
Na ₂ O	0.00	± 0.00	0.01	± 0.01	0.06	± 0.01	0.00	± 0.00	0.38	± 0.00	0.01	± 0.00
Total	100.87	± 0.48	100.31	± 0.50	99.65	± 0.65	97.09	± 1.72	100.33	± 1.00	100.23	± 0.23
Molar Cations	Olivine 3		OPX 4		Augite 4		Chromite 3		Plagioclase 5		Dunite bulk Calculated	
Si	0.996		1.939		1.917		0.020		2.030			
Ti	0.001		0.015		0.032		0.042		0.000			
Al	0.002		0.063		0.096		0.459		1.952			
Cr	0.001		0.017		0.024		1.400		0.000			
Fe	0.335		0.296		0.135		0.770		0.026			
Mn	0.004		0.006		0.004		0.012		0.000			
Mg	1.659		1.610		0.935		0.283		0.008			
Ca	0.002		0.053		0.854		0.014		0.949			
Na	0.000		0.000		0.004		0.000		0.034			
Mg*	83.2		84.5		87.4		26.9				83.1	
Wo			2.7		44.4							
En			82.2		48.6							
Fs			15.1		7.0							
An									96.5			

Notes: See Online Materials' spreadsheet for details and individual analyses. Uncertainties are 1σ. Mg* is molar Mg/(Mg+Fe) in %; In pyroxenes, Wo is molar proportion CaSiO [molar % Ca/(Ca+Mg+Fe)], and En is molar proportion MgSiO₃ [molar % Mg/(Ca+Mg+Fe)]. An is molar Ca/(Ca+Na) in %.

al. 2010; Klima et al. 2011; Kramer et al. 2013; Moriarty et al. 2013, 2021b; Corley et al. 2018; Gou et al. 2019; Lemelin et al. 2019; Li et al. 2019; Bretzfelder et al. 2020; Gou et al. 2020). However, mineralogy and mineral compositions determined by remote sensing do not permit determination of pressures and temperatures of equilibration.

Lunar dunites

There are few dunites and peridotites in the returned lunar sample collection. Only one macroscopic dunite was collected by the Apollo astronauts, 72415 (and its pairs), and peridotitic fragments are known in only a few lunar breccia rocks.

The only large sample of lunar dunite, 72415 to 72418, was a clast in a fragmental melt breccia, exemplified by sample 72435 (Meyer 2012). 72415 is a cataclastic breccia, composed primarily of olivine fragments (up to 10 mm across) in a matrix of granulated olivine with small proportions of high- and low-Ca pyroxenes, plagioclase, chromite, and others (Dymek et al. 1975). 72415 has been interpreted as nearly monomict, with rare fragments of chromite-pyroxene symplectites and impactites (Dymek et al. 1975). Olivine in 72415 has a small range in composition, Fo₈₆₋₈₉ [the Fo number is atomic Mg/(Mg+Fe) in %, see Table 1], and two-pyroxene thermometry implies equilibration at 1120 °C (Ishii et al. 1976). The source of 72415 (mantle or crust) is discussed below.

Approximately a dozen fragments of dunite and peridotite have been recognized in Apollo 14 breccias (Taylor and Marvin 1971; Lindstrom et al. 1984; Shervais et al. 1984; Goodrich et al. 1986; Warren et al. 1987; Morris et al. 1990; Snyder et al. 1995; Shervais and McGee 1999). These olivine-rich rocklets are all magnesian and variably enriched in KREEP component. For the most part, they have been interpreted as crustal cumulates from Mg-suite magmas. The Apollo 14 breccias also contain a few complex peridotitic

fragments, one of which is interpreted as asteroidal (Shervais et al. 1984). The others are likely to be fragments of crustal cumulate rocks (Taylor and Marvin 1971; Morris et al. 1990).

A few dunite fragments are reported from Apollo 15 regolith breccias (Marvin et al. 1989a, 1989b, 1991). Marvin and colleagues suggested that these fragments formed at significant depth, but did not distinguish between a crustal and mantle origin.

Finally, the Apollo 17 basalt 74275 contains xenoliths of dunite (Shearer et al. 2015a). The xenoliths' olivine cores retain igneous-like zoning patterns in Al, Ti, and P; this zoning led Shearer et al. to infer a shallow crustal origin. However, similar chemical zoning has recently been recognized in the troctolite 76535 (Nelson et al. 2021), which is inferred to have formed at depth and cooled slowly, see Figure 4 here and McCallum and Schwartz (2001).

Meteorites

Among lunar meteorites, only a few dunitic and peridotitic clasts have been reported in regolith or melt breccias; no lunar meteoritic dunites (or dunitic peridotites) are known. In meteorite ALH 81005, despite extensive study of many thin sections, only a few peridotitic fragments have been reported (Kurat and Brandstätter 1983; Warren et al. 1983; Brum 2022; Brum et al. 2022). Dunitic and peridotitic material are absent to uncommon in other lunar meteorites (Warren et al. 1983; Arai et al. 2002; Nazarov et al. 2004; Sugihara et al. 2004; Hudgins et al. 2007; Bischoff et al. 2010; Mercer et al. 2013; Cao et al. 2020; Bechtold et al. 2021). Many of these fragments have moderate Mg*, and are likely related to the lunar Mg-suite (Shearer et al. 2015b).

NWA 8046 clan

Here, we present a clast of dunite in lunar meteorite Northwest Africa (NWA) 11421, which is a member of the NWA 8046 clan

of lunar highlands breccias, the “Algerian Megafind” (Korotev 2022). These tens of named meteorites are paired, being either all fragments of the same meteoroid fall, or being “source paired” in coming from the same site on the Moon. The most detailed published description of NWA 8046 meteorite is for NWA 11460 by Cao et al. (2021). Their description is consistent with our observations of NWA 11421.

A dunite clast is also present in NWA 14900 (Sheikh et al. 2022), a member of the NWA 8046 clan (Korotev 2022). This fragment consists only of olivine (Fo₉₁) with a miniscule proportion of chromite. No other studies of NWA 8046 meteorites mention clasts of dunite, peridotite, or other ultramafic materials (Lunning and Gross 2019; Fagan and Gross 2020; Zeng et al. 2020; Treiman and Semprich 2021; Saini et al. 2022).

SAMPLES AND METHODS

Samples

A piece of NWA 11421, 11.67 g, was purchased from M. Cimala of Polandmet.com (Fig. 1). The properties of this fragment are consistent with the official description of the meteorite (Gattacceca et al. 2019). NWA 11421 a member of the NWA 8046 clan of impact melt breccias, which consist of mineral and lithic fragments (mostly anorthositic troctolite or lherzolite) in dense black glass, see Figure 1 (Treiman and Coleff 2018; Cao et al. 2021; Korotev 2022). The dunite clast studied here, D1 (Fig. 1), was noted on a weathered surface by its color, and its extent determined with X-ray computed tomography, XCT, see Figure 2 (Treiman and Coleff 2018). Based on the XCT, the sample was cut to produce two thick sections (labeled NWA 11421_lpi1 and _lpi2) that expose the dunite clast (NWA 11421_lpi1_D1), leaving a significant portion of it remaining in the meteorite fragment. The results here are all from NWA 11421_lpi1.

Methods

Electron microbeam. The dunite D1 and its surroundings in thick section NWA 11421_lpi1 were imaged in backscattered electron (BSE) mode using the JEOL 7600F at the Astromaterials Research and Exploration Science (ARES) Division, Johnson Space Center, Houston, Texas and with the PhenomXL SEM at the Lunar and Planetary Institute (USRA), Houston, Texas. Qualitative maps of element abundances (by energy-dispersive spectrometry, EDS), were acquired with the



FIGURE 1. A portion of the NWA 11421 fragment investigated here, macroscopic visible-light, true color. The meteorite consists of lithic clasts in dark glassy matrix. The studied dunite clast (D1) at the image center is brown, 0.7 cm long. In it, olivine is pale brown, orthopyroxene is darker brown, and augite is dark green. Most other visible clasts are troctolitic (t, plagioclase + olivine). Photo courtesy of M. Cimala (polandmet.com).

same instruments. Based on these element mappings, selected spots were chosen for quantitative chemical analysis using the JEOL 8530 FEG electron microprobe (EMP) at ARES. Analytical conditions were nominal for the instrument and laboratory. Peak intensities were measured for $K\alpha$ radiation of these elements using well characterized standards: Si, diopside; Ti, rutile; Al, oligoclase; Cr, chromite; Fe, fayalite; Ni, NiO; Mn, rhodonite; Mg, diopside or forsterite; Ca, diopside; Na, oligoclase; K, orthoclase; and S, anhydrite. The incident electron beam was at 15 kV and 10 nA (for plagioclase) or 25 nA (for other minerals) measured in a Faraday cup, and was focused on surfaces of standards and samples. Peak X-ray intensities were counted for 30–60 s, and backgrounds were counted for the same total durations. Analytical standards were run as unknowns to validate the calibrations.

All mineral analyses and their locations on the thick section are given in the Online Materials¹.

Mineral proportions, densities, and bulk composition. Mineral proportions in the dunite clast D1 were calculated using a supervised classification routine on element abundance images from the SEM. The classification was done using the Multispec program (Landgrebe and Biehl 2011) following the protocols of Maloy and Treiman (2007). X-ray element images were masked to include only the D1 clast; mineral classification training was based on EMP quantitative point analyses. Mineral densities (at 1 bar) were calculated assuming linear mixing from the densities of end-member compositions.

D1's bulk composition was calculated from the area proportion of each phase in it (olivine, orthopyroxene, clinopyroxene, plagioclase, chromite), the point EMP analyses of each phase, and the calculated densities of each.

X-ray computed tomography (XCT). An X-ray tomography image stack of the whole meteorite piece was acquired at the ARES division of Johnson Space Center in May 2018 (Treiman and Coleff 2018). The XCT instrumentation and methods are as described in Zeigler et al. (2017) and Eckley et al. (2020); see Online Materials¹ Appendix I.

Thermobarometry. Details of the thermobarometry calculations are given in the text below and in Online Materials¹ Appendix II, including mineral analyses on which they are based,

RESULTS

The analyzed section of NWA 11421 is a lunar highlands melt breccia (Figs. 1, 2, and 3) consistent with its classification (Gattacceca et al. 2019) and its pairing into the NWA 8046 clan (Korotev 2022). Most of the lithic fragments in the section are troctolitic or lherzolitic anorthosites (Figs. 2d and 3a); there are also clasts of anorthositic impact melt and breccia. No basaltic or KREEPy fragments have been noted, although the rock contains rare small fragments of evolved, silica-rich material (Treiman and Semprich 2019). Mineral grains include those from the anorthositic and dunitic lithologies, and other types including exsolved low-Ca and high-Ca pyroxenes, Fe-sulfide, Fe-metal, and Mg-Al spinel (Fig. 3a).

The thick section _lpi1 (and the meteorite in general) shows minor evidence of terrestrial weathering (Korotev 2022). One crack in the D1 dunite and its surroundings contains K-rich material, tentatively identified as clay (Fig. 3c). Another crack contains a Ca-rich grain (Fig. 3c), without other elements detectable by EMP, that is likely a Ca-carbonate. That same crack also contains a sulfur-bearing grain, again without elements detected in our EMP maps (Fig. 3c). This could be a grain of barium sulfate (barite), such as occurs in other NWA meteorites (Korotev et al. 2009).

Dunite mineralogy and composition

The D1 dunite fragment, before cutting, was approximately $10 \times 7 \times 4$ mm (Figs. 1 and 2). The thick section analyzed here exposes a 5×4 mm surface of the dunite (Fig. 3). The thick-section surface appears representative of the whole fragment, except that it does not expose an apparent stringer of high-density

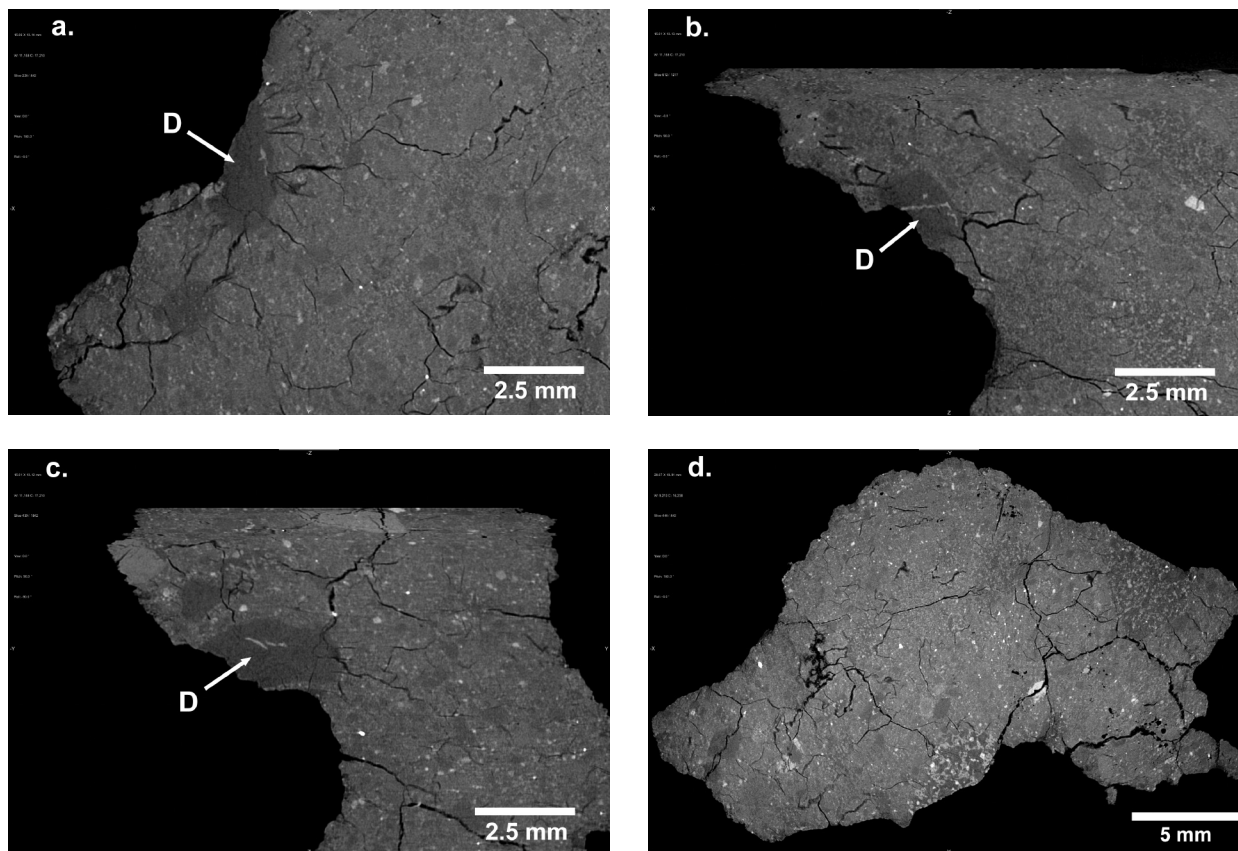


FIGURE 2. X-ray computed tomogram (XCT) slices of the NWA 11421 piece. (a) Parallel to the base of the sample (in Fig. 1), cutting through the dunite clast (D). Note other dark, plagioclase-rich clasts and speckled matrix (devitrified impact melt). (b) XCT slice perpendicular to that of 1a, bottom of the sample to top of image, and partially distorted. Dunite (D) cut by bright veinlet, possibly rich in chromite symplectite. (c) XCT slice perpendicular to those of Figures 1a and 1b, bottom of the sample to top of image, and partially distorted. Dunite (D) cut by bright discontinuous veinlets. (d) General XCT view of meteorite, slice parallel to that of Figure 1a, but away from the dunite. Note coarser grained clasts of plagioclase-rich (dark areas) troctolite and ilherzolite in fine-grained speckled matrix (devitrified impact melt).

material visible in the XCT scan (Figs. 2b and 2c).

Mineralogically, the D1 dunite is simple; it consists only of olivine, low-Ca pyroxene, high-Ca pyroxene, anorthite plagioclase, and chromite (Fig. 3a). No other phases were detected (Fig. 3), such as Fe ± Ti oxides, Ca-phosphates, zircon/baddeleyite, alkali feldspar, or garnet. A small proportion of K-bearing material on a fracture (Fig. 3c) is interpreted as clay produced during terrestrial weathering. Minerals in the dunite are nearly of constant compositions and lack zoning in major or minor elements (Fig. 4); Table 1 gives average mineral compositions, and a calculated bulk composition of the dunite (based on mineral proportions, analyses, and densities; Table 2); full analyses are in the Online Materials¹.

The silicate minerals are magnesian; the olivine is Fo₈₃ (Fig. 4; Table 1), and the pyroxenes are slightly more magnesian (Wo₀₃En₈₂Fs₁₅ and Wo₄₄En₄₉Fs₀₇, Table 1), consistent with Fe-Mg equilibria (Baker and Herzberg 1980; Lindsley 1983). The olivine has FeO/MnO = 84, consistent with a lunar provenance (Karner et al. 2003). The pyroxenes contain minor non-quadrilateral components (e.g., Al, Ti, Cr, Na), and so are represented well on a standard pyroxene quadrilateral (Fig. 4). The augite is slightly

sub-calcic, and the orthopyroxene contains a small proportion of Ca (Table 1; Fig. 4). D1's plagioclase is An_{96.5} (see Table 1 for values and abbreviations), such as is abundant in lunar anorthosites and most lunar rocks. Its chromite is a complex solid solution, with significant Al substitution for Cr, Mg substitution for Fe²⁺, and a small proportion of Ti. The analytical sums for chromite are low, which we attribute to its small grain size and irregular surfaces near grain edges; the chromite standard analyzed well. It is also possible that the dunite's chromite contains an unanalyzed element or a bit of ferric iron.

Mineral proportions and their calculated densities are given in Table 2, along with a calculated bulk density for the D1 dunite.

Dunite texture

Macroscopically, the D1 dunite has a granoblastic-polygonal texture, and lacks apparent preferred mineral orientations. This absence of preferred orientations is also seen on the weathered meteorite surface (Fig. 1), in the different colors of the olivine, augite, and orthopyroxene grains. Note that the weathered and cut surfaces are approximately perpendicular to each other. Likewise, the XCT scan shows no alignments or preferred ori-

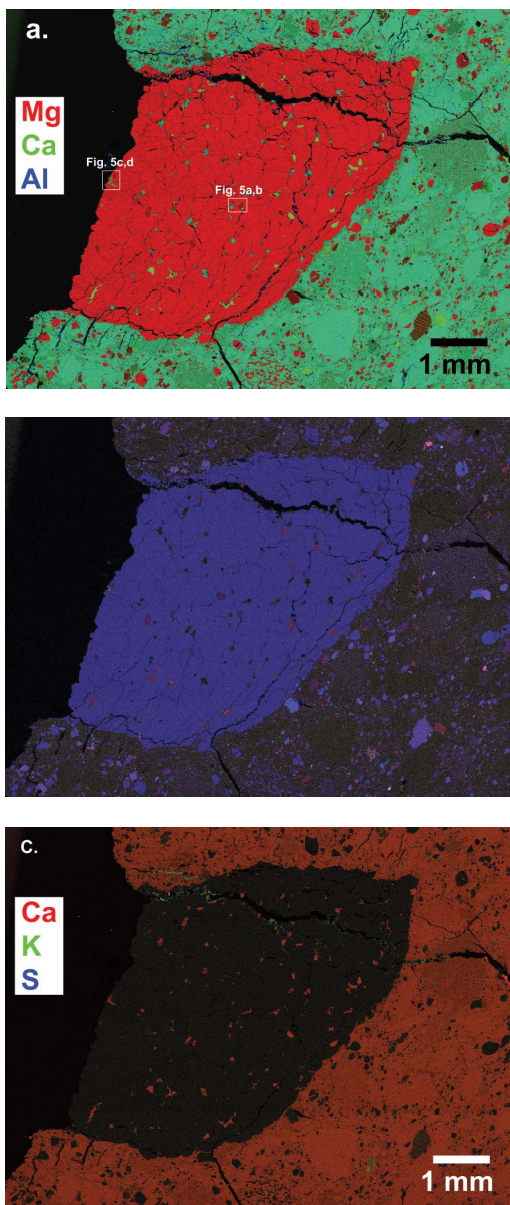


FIGURE 3. Multi-element images, by SEM/EDS of the D1 dunite clast and surroundings. Epoxy is black in all frames (left of the rock sample, and filling cracks across it). (a) Mg-Ca-Al, showing main minerals in clast, and their chemical homogeneity. In the dunite clast: bright red is olivine; dull red is orthopyroxene; green is augite; blue-green is plagioclase, and small discrete black spots in the dunite are chromite. White rectangles are locations of images in Figure 5. The matrix, being rich in plagioclase, is dominantly blue-green. (b) Ti-P(Zr)-Fe. $PK\alpha$ and $ZrL\alpha$ X-rays are not distinguished. The dunite and many mineral fragments in the matrix contain Fe (in blue). Chromite in the dunite is magenta, as is ilmenite in the matrix. A few spots in the matrix, greenish and white, could be Ca-phosphate, zircon, or baddeleyite. (c) Ca-K-S, shows weathering products along cracks. Ca-rich spots along a crack (bright red, far right center) are interpreted as calcite; K-bearing streaks and veinlets (green) are interpreted as clay minerals. A few S-rich grains (blue) along cracks (S, but no Ca) could be barite; S-rich spots in the matrix are Fe-sulfides. The small greenish clast (K-bearing) left of the scale bar is one of the few evolved rock fragments in the meteorite (Treiman and Semprich 2021).

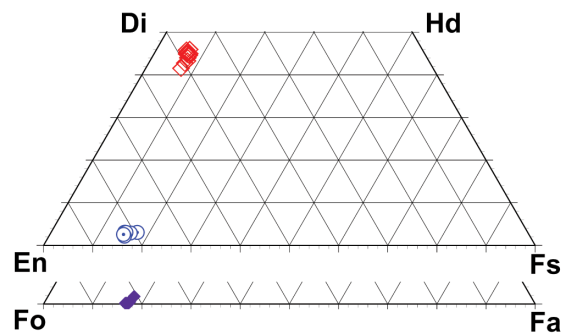


FIGURE 4. Pyroxene and olivine compositions in the D1 dunite. Pyroxene end-members are: En = enstatite ($Mg_2Si_2O_6$); Fs = ferrosilite ($Fe_2Si_2O_6$); Di = diopside ($CaMgSi_2O_6$); Hd = hedenbergite ($CaFeSi_2O_6$). Olivine end-members are: Fo = forsterite (Mg_2SiO_4); Fa = fayalite (Fe_2SiO_4); Ca-olivine (Ca_2SiO_4). Compositions of augite (open red squares), orthopyroxene (dotted blue circles), and olivine (filled purple diamonds) are nearly constant across the dunite clast. The range of Wo content of the augite could represent slight mixture with orthopyroxene.

TABLE 2. Mineral proportions and densities

Mineral	Area %	Density kg/m ³
Olivine	95.3	3380
Augite	1.1	3250
Orthopyroxene	1.6	3400
Plagioclase	1.3	2730
Chromite	0.7	5000
Bulk dunite		3380

entations of the pyroxene and plagioclase grains (Fig. 2). Thus, we infer that the dunite lacks linear and/or planar structures; i.e., it is structurally isotropic.

Olivine grains can be distinguished from each other, at least in part, by the presence of gaps (from grinding/polishing) along grain boundaries and cracks representing cleavage in individual grains (Figs. 3 and 5). From this view, the D1 olivines are all of approximately the same size, $\sim 100 \mu m$ across, and show no obvious preferred elongation direction. Boundaries between grains of olivine (as can be discerned) are generally planar (Fig. 5) and are consistent with triple-junction angles of $\sim 120^\circ$.

Pyroxenes and plagioclases appear randomly distributed among the olivine grains, Figure 3a, and few of these appear elongated or aligned. The few elongated augite grains (e.g., bottom left of the clast in Fig. 3a) are associated with augite-chromite symplectites and are inferred to be late-stage additions (see below). Boundaries of pyroxene and plagioclase grains against olivines are either straight or concave toward the olivine (Fig. 5), consistent with inferred constraints of equilibrium surface energy (Spry 1969; Barker 2013).

Symplectite

Chromite and some augite in the D1 dunite are exceptions to this textural equilibrium. Nearly all the chromite occurs either as symplectic intergrowths with augite (Figs. 5c and 5d) or elongate grains, sandwiched between silicate mineral grains. Much of the augite is in equant anhedral grains (e.g., Fig. 3a, upper right side of dunite clast), but some augite is in symplectic intergrowths with chromite (Figs. 5c and 5d), and some occurs as elongate grains between other mineral grains (e.g., at the center of Fig. 5b).

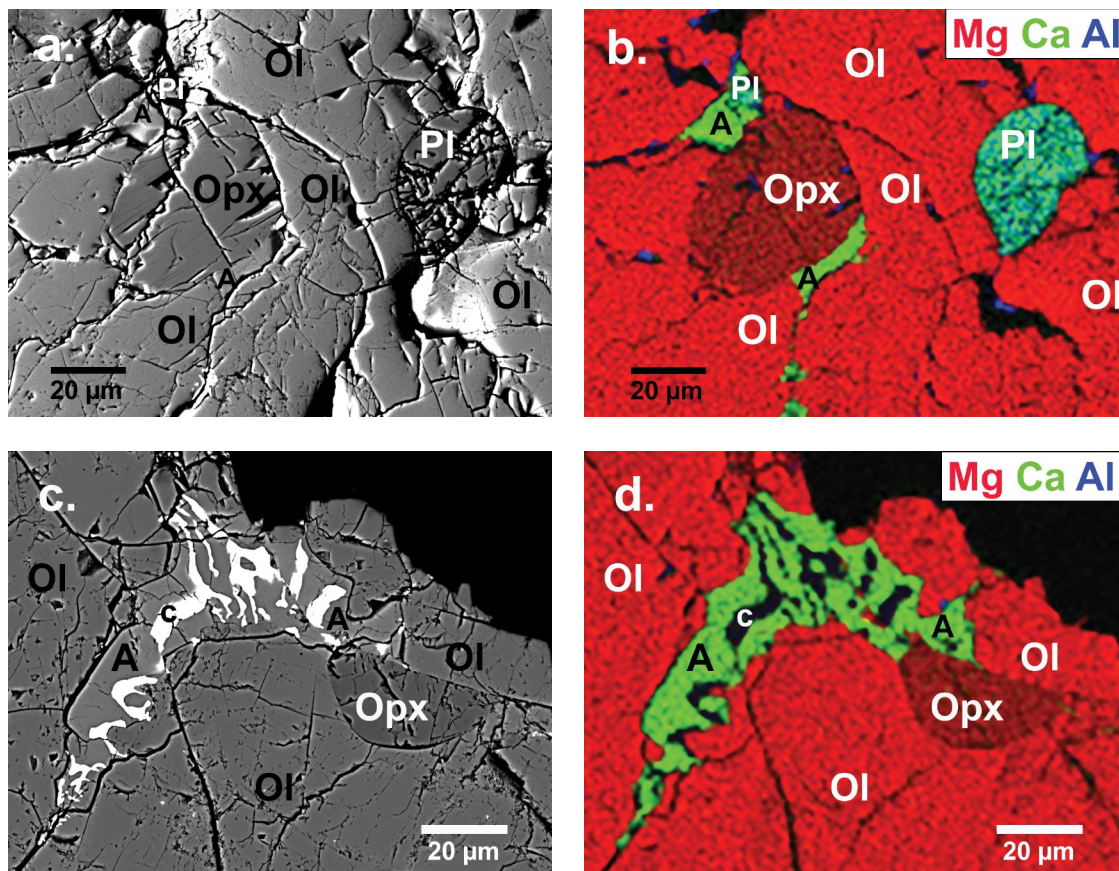


FIGURE 5. Details of textural relationships in the D1 dunite. (a) BSE image of typical dunite texture: olivine (Ol, bright red), plagioclase (Pl, teal), augite (A, green), and orthopyroxene (Opx, dull red). The individual grains are in textural equilibrium, except for the elongate augite (see c and d). (b) Mg-Ca-Al element map of same area. Enlarged by interpolation from Figure 3a. Al-rich areas (bright blue) are traces of alumina polishing compound in cracks. (c) BSE image of largest augite-chromite symplectite; mineral labels as above plus chromite (c). (d) Mg-Ca-Al element map of same area as c. Enlarged by interpolation from Figure 3a.

The largest example of elongated grains in the thick section is in the lower left corner of the dunite in Figure 3a. There, an elongate augite grain and an augite-chromite symplectite define a short veinlet cutting the dunite. This veinlet could be an example of the high-density veinlets observed in XCT (Figs. 2b and 2c).

INFERENCES

Thermobarometry

The mineral compositions in the NWA 11421_lpi1_D1 dunite appear to represent a state of chemical equilibrium, so we can apply thermobarometry to determine its equilibrium temperature and pressure. We consider the minerals to be in chemical equilibrium first because the compositions of each mineral are consistent across the dunite fragment (Fig. 4; Online Materials¹); second because the Mg*s of the olivine, augite, and orthopyroxene are consistent with equilibrium, see Table 1 and Figure 4 (Baker and Herzberg 1980; Lindsley 1983); and finally because the Ca contents of the augite and orthopyroxene are consistent with equilibrium (Lindsley 1983).

With this evidence of chemical equilibrium, we can apply

established mineral thermobarometers to determine the temperature and pressure at which the dunite's minerals equilibrated: 980 ± 20 °C and 0.4 ± 0.1 GPa. We calculated temperatures and pressures for six different sets of minerals (Ol + Pl + Cpx + Opx) in direct or nearly direct contact, Figure 6 (see Online Materials¹). Details of the temperature and pressure calculation are given in Online Materials¹ Appendix II. Equilibration temperatures were calculated from two-pyroxene thermometry (Ca distribution between augite and orthopyroxene) using the calibration of Brey and Köhler (1990) and two calibrations from Putirka (2008). For each set of minerals, these temperatures are within 20 °C of each other. The resulting minimum and maximum temperatures were then used as input to calculate pressures using THERMOCALC's avP algorithm (Powell and Holland 1994, 2008), selecting the temperature that produced the P result with the lowest residuals. The calculated pressures rely primarily on the Al contents of pyroxenes, e.g., the Mg- and Ca-Tschermak's, or kushiroite (Kimura et al. 2009), components. To validate the procedure, we calculated temperatures and pressures for the lunar troctolite 76535 (Fig. 6; Online Materials¹ Appendix II); our results are comparable to those in earlier studies (McCallum and Schwartz

2001; Elardo et al. 2012). For the six sets of minerals in the D1 dunite, calculated equilibrium temperatures range from 940 to 990 °C (Fig. 6), with an average of 980 °C. Calculated equilibrium pressures range from 0.27 ± 0.1 to 0.51 ± 0.1 GPa (Fig. 6), with a best estimate of 0.4 ± 0.1 GPa.

Equilibration depth: The upper mantle

To understand the original geologic setting of the NWA 11421_lpi1_D1 dunite, it is crucial to know how the calculated equilibrium pressure corresponds to depth. We use the Wieczorek et al. (2013) model of the lunar crust and upper mantle: a porous (fragmented) anorthositic crust with average density of 2550 kg/m^3 and thickness from 34 to 43 km, overlying a peridotitic upper mantle of density 3400 kg/m^3 (nearly identical to that calculated for the dunite, Table 2). With those constraints (and lunar surface gravity of 1.62 m/s^2), pressure at the base of the crust is calculated to be 0.14 to 0.18 GPa. The equilibration pressure for D1 is greater than these pressures, which places D1's equilibration in the Moon's upper mantle. Using the Wieczorek et al. (2013) model, the D1 dunite equilibrated at a depth of $88 \pm 22 \text{ km}$ in the Moon's upper mantle.

The dunite's mineral equilibration is consistent with formation on a "normal" present-day lunar geotherm (i.e., selenotherm), see Figure 7. Within 2σ uncertainty, the dunite's equilibration is consistent with the present-day selenotherm calculated by Khan et al. (2014) from seismic data. That selenotherm includes consideration of a partially molten mantle at depths $>1200 \text{ km}$, and a porous crust of low thermal conductivity. The nominal pressure and temperature of equilibration plot at slightly higher temperature (or lower pressure) than Khan's selenotherm (Fig. 7), consistent also with equilibration along an ancient, slightly hotter, thermal gradient.

Texture

The texture of the D1 dunite (excepting the symplectites) arose during its chemical and thermal history in the Moon, and so reveals some of that history. As described above, olivine grains in

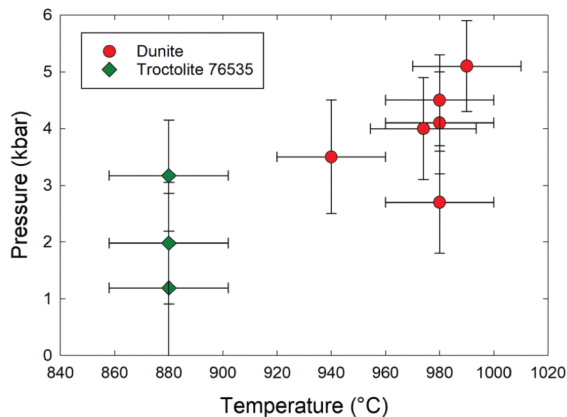


FIGURE 6. Calculated temperatures and pressures for separate mineral groups in the D1 dunite, red circles (see Online Materials¹ Appendix II and Online Materials¹) and clinopyroxene-olivine pairs in lunar troctolite 76535, green diamonds (see Online Materials¹ Appendix II). Standard deviations are 1σ .

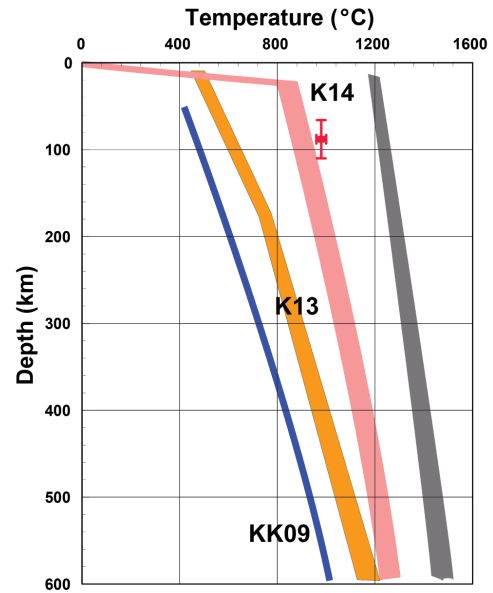


FIGURE 7. Equilibration conditions of the NWA 11421_lpi1_D1 dunite, and present-day thermal trajectories in the lunar mantle, after Figure 2 of Garcia et al. (2019). Equilibrium p-T in red (Fig. 6), with 1σ uncertainties. Pink band (K14) covers best model selenotherms of Khan et al. (2014), which include 40 km thick, porous crust of low thermal conductivity. Orange band (K13) includes calculated selenotherms for dry olivine \pm orthopyroxene from Karato (2013); blue line (KK09) is selenotherm from Kuskov and Kronrod (2009). Gray band includes estimates of the solidus for undifferentiated lunar mantle material (Longhi 2006; Hirschmann 2000).

D1 are all of approximately the same size (Fig. 3), and show no obvious elongations or preferred orientations. None of the minerals in D1 show their own crystal forms (i.e., are not idiomorphic); rather, grain boundaries are straight or curved as consistent with equilibria of mineral surface energies (Spry 1969).

These textures of D1 are consistent with those of a granoblastic-polygonal metamorphic rock—one in which grain sizes and boundaries have adjusted to equilibrium shapes during extensive thermal metamorphism without deformation. Granoblastic-polygonal textures are common among mantle rocks from the Earth (Mercier and Nicolas 1975), although Earth mantle rocks tend to have larger grains (e.g., $\sim 1 \text{ mm}$ vs. the 0.1 mm of D1). Such textures are not characteristic of igneous cumulate rocks (Wager et al. 1960; Wager and Brown 1967).

Symplectite formation

The chromite-augite symplectites in the D1 dunite require explanation in the context of long-standing controversies about symplectite formation in other lunar rocks. In the still-current summary, Bell et al. (1975) described six varieties of lunar symplectites and four general formation mechanisms. The symplectites in D1 fall into Bell's category C, "... 10–1000 μm elongated masses along grain boundaries..." (Figs. 5c and 5d). Bell and coauthors agreed that type-C symplectites are formed by reactions between olivine and plagioclase. Dymek et al. (1975) inferred that similar symplectites in 72415 were formed by in-

teraction with a silicate fluid (i.e., in an open system). Elardo et al. (2012) confirmed this inference, showing that symplectites of this type in troctolite 76535 (their Fig. 1) formed by the addition of Cr and Fe in an open-system process. The D1 symplectites are similar enough to those in 76535 (Elardo et al. 2012) in texture and in composition that a similar open system origin seems reasonable. An origin by garnet breakdown seems unlikely for the D1 symplectites because garnet in peridotites tends to form euhedra (Spry 1969; Dégi et al. 2010; Barker 2013) and not intergranular pods and films (Figs. 2b, 2c, 3a, 5c, and 5d).

The lunar upper mantle

It seems presumptuous to extrapolate from a single clast in a breccia to the Moon's whole mantle, yet such assumptions have proven useful (Wood et al. 1970). If the D1 dunite clast in NWA 11421 is representative of a portion of the lunar mantle, it could help constrain models of the Moon's early history.

The Al, Ca, and Ti abundances in the D1 dunite seem most consistent with formation in a differentiated lunar mantle that was well mixed after its overturn (see Introduction). Estimated compositions of the bulk, undifferentiated lunar mantle have 3–7% Al₂O₃, 3–5% CaO, and 0.2–0.4% TiO₂ (Elkins-Tanton et al. 2011), while the dunite contains only 0.55% Al₂O₃, 0.57% CaO, and 0.07% TiO₂ (Table 1). Thus, the dunite composition is consistent (in general terms) with a primitive mantle composition that was depleted in components that partition into silicate melt (e.g., Al, Ca, Ti).

The dunite's Mg* (i.e., Fo) of 83 is consistent with most models of the bulk primitive lunar mantle, which have Mg* = 80–85; see Table 1 of Elkins-Tanton et al. (2011). A lunar mantle that differentiated during a magma ocean episode would retain that average bulk Mg* and be stratified with the highest Mg* at its base (according to mineral-melt element partitioning). In some models of LMO crystallization, Fo₈₃ olivine is calculated to form only after ~65–75% of LMO crystallization (depending on the model starting composition), and is nearly the last olivine to crystallize (Elkins-Tanton et al. 2011; Lin et al. 2020; Johnson et al. 2021). In other models of LMO crystallization Fo₈₃ olivine does not crystallize (Snyder et al. 1992; Rapp and Draper 2018); low-Ca pyroxene would be the only silicate with Mg* = 83.

This cumulate pile from a crystallizing LMO would have been gravitationally unstable, having the Fe-rich denser materials near the top. This pile would have overturned, bringing denser material to the mantle base with some degree of mixing (Hess and Parmentier 1995). If there had been no mixing after overturn, e.g., Figure 5b of Elkins-Tanton et al. (2011), olivine at the depth inferred for the NWA 11421 dunite would be ~Fo₉₀, significantly more magnesian than observed (Table 1). This mismatch in Fo number implies that at least some of the lunar mantle had been mixed during overturn. However, the presence of augite-chromite symplectites that post-date dunite formation (see below) allows the possibility that the original dunite might have been somewhat more magnesian than what we now see, having equilibrated with the Fe-Cr-bearing material responsible for the symplectites.

If a stratified differentiated lunar mantle had homogenized during or after overturn (Boukaré et al. 2018; Zhao et al. 2019), then it would maintain its bulk Mg* across all depths and so

would be consistent with the Mg* and inferred depth for the NWA 11421 dunite (Table 1). Likewise, abundances of Al and Ti in the dunite are consistent with a differentiated mantle, one from which igneous, incompatible elements had been partially removed to form the lunar anorthositic crust and incompatible-enriched late LMO melts. So, the NWA 11421 dunite is most consistent with a lunar mantle that was mixed well after (or during) its overturn (Boukaré et al. 2018; Moriarty et al. 2021a).

DISCUSSION: OTHER POSSIBLE SAMPLES OF THE LUNAR MANTLE

To our knowledge, D1 in NWA 11421 is the first lunar sample known to have equilibrated at pressures consistent with the lunar mantle. It is possible that other lunar dunites and peridotites are samples of the lunar mantle, but few are reported to have mineral assemblages (olivine-plagioclase-augite-low-Ca pyroxene) that could provide equilibration temperatures and pressures (see Online Materials¹ Appendix II). See Online Materials¹ Appendix III for comments about thermobarometry of lunar spinel cataclasesites.

However, many lunar symplectites have bulk compositions consistent with mixtures of garnet ± olivine (Bell et al. 1975), which suggests that they were originally those minerals and decomposed to augite + chromite on decompression (Bell et al. 1975; Schmitt 2016). Specifically, symplectites in dunite 72415 have been interpreted as products of the decomposition of garnet (Schmitt 2016; Bhanot et al. 2022). If so, the garnet must have originated in the lower lunar mantle at pressures greater perhaps than 2.3 GPa (Schmitt 2016). The garnet would then have been transported, perhaps during the overturn of the LMO cumulates, to the shallow mantle (Bhanot et al. 2022), where it could have decomposed to symplectites and then would have been transported to the surface.

IMPLICATIONS

The D1 dunite clast in NWA 11421_lpi1 equilibrated last at ~980 °C and 0.4 ± 0.1 GPa, at a depth of 88 ± 22 km, firmly in the Moon's upper mantle. This temperature and pressure are consistent with estimates of the present-day selenotherm (Khan et al. 2014). Its chemical composition (Mg*, Al content) is consistent with estimates of the bulk composition of the lunar mantle, suggesting that the dunite formed after mantle differentiation (separation of anorthositic crust and Fe-Ti-rich residua) and after density-driven overturn re-homogenized mantle. This interpretation of the D1 dunite's origin is not unique—a similar chemistry and texture could form from an undifferentiated mantle composition by the removal of a partial melt or perhaps a garnetiferous peridotite.

The veinlets and masses of augite and augite-chromite symplectite represent a fluid-based metasomatic event after the dunite host had achieved textural equilibrium (presumably still in the mantle). Similar metasomatic products occur in other lunar and asteroidal samples (Elardo et al. 2012; Vaci et al. 2021), and their origin remains unclear, especially the nature and origin of the metasomatic fluid.

The D1 dunite is the first recognized sample of the lunar mantle, although mantle rock is inferred to have been brought to the surface by large impact events (Yamamoto et al. 2010; Miljković et al. 2015; Bretzfelder et al. 2020; Moriarty et al.

2021a). It is puzzling that no other bits of mantle dunite have been recognized, despite the relative abundance of crustal-intrusive rocks in the meteorite and Apollo collections, e.g., McCallum and Schwartz (2001) and Elardo et al. (2012). Finding other fragments of lunar mantle rock would be very useful, and the search should be widened. The clast described here was recognized first because it was exposed on a weathered surface; where possible, XCT scans of other lunar breccias could reveal more fragments of the lunar mantle.

ACKNOWLEDGMENTS AND FUNDING

We are grateful to M. Cimola for availability of the meteorite sample, and for providing the original of Figure 1. We are grateful to K. Ross for assistance with the EMP analyses, and to C. Goodrich for some of those analyses. D. Coleff and R. Zeigler assisted with the XCT scan. Reviewer comments and corrections from J. Gross, A. Ruzicka, D. Shiekh, H. Downes, and an anonymous reviewer are deeply appreciated. The Phenom SEM at the Lunar and Planetary Institute (LPI) was purchased with funds from USRA's IR&D fund. The LPI is operated by Universities Space Research Association (USRA) under a cooperative agreement with the Science Mission Directorate of NASA. The thick section NWA 11421_lpi1 with the dunite clast D1 is curated at the XSPACE archive at the Lunar and Planetary Institute (<https://www.lpi.usra.edu/science/science-labs-equipment/xspace/>). LPI Contribution 3008.

REFERENCES CITED

- Arai, T., Ishi, T., and Otsuki, M. (2002) Mineralogical study of new lunar meteorite Yamato 981031. *Lunar and Planetary Science Conference 33rd*, 33, 2064.
- Baker, M.B., and Herzberg, C.T. (1980) Spinel cataclases in 15445 and 72435—Petrology and criteria for equilibrium. *Lunar and Planetary Science Conference Proceedings*, 11, p. 535–553.
- Barker, A.J. (2013) Introduction to Metamorphic Textures and Microstructures, 290 p. Stanley-Thornes.
- Bechtold, A., Brandstätter, F., Pittarello, L., Ferrière, L., Greenwood, R.C., and Koeberl, C. (2021) Lunar meteorite Northwest Africa 11962: A regolith breccia containing records of titanium-rich lunar volcanism and the high alkali suite. *Meteoritics & Planetary Science*, 56, 971–991, <https://doi.org/10.1111/maps.13659>.
- Bell, P.M., Mao, H.K., Roedder, E., and Weiblen, P.W. (1975) The problem of the origin of symplectites in olivine-bearing lunar rocks. *Proceedings, Lunar Science Conference 6th*, p. 231–248.
- Bhanot, K.K., Downes, H., Jennings, E., and Wotton, S. (2022) Apollo 17 Sample 72415—A Fragment of the Lunar Mantle? 53rd Lunar and Planetary Science Conference, p. Abstract 1820. Lunar and Planetary Institute, Houston.
- Bischoff, A., Horstmann, M., Pack, A., Laubenstein, M., and Haberger, S. (2010) Asteroid 2008 TC3—Almahata Sitta: A spectacular breccia containing many different ureilite and chondritic lithologies. *Meteoritics & Planetary Science*, 45, 1638–1656, <https://doi.org/10.1111/j.1945-5100.2010.01108.x>.
- Boukaré, C.-E., Parmentier, E., and Parman, S. (2018) Timing of mantle overturn during magma ocean solidification. *Earth and Planetary Science Letters*, 491, 216–225, <https://doi.org/10.1016/j.epsl.2018.03.037>.
- Bretzfelder, J.M., Klima, R.L., Greenhagen, B.T., Buczkowski, D.L., Petro, N.E., and Day, M. (2020) Identification of potential mantle rocks around the lunar Imbrium basin. *Geophysical Research Letters*, 47(22), e2020GL090334.
- Brey, G.P. and Köhler, T. (1990) Geothermobarometry in four-phase Iherzolites II. New thermobarometers, and practical assessment of existing thermobarometers. *Journal of Petrology*, 31, 1353–1378, <https://doi.org/10.1093/ptrology/31.6.1353>.
- Brum, J.T. (2022) New insights into the petrogenesis of lunar meteorite Allan Hills 81005 (ALHA81005). *Geology and Environmental Earth Science*, M.S. thesis, 72. Miami University.
- Brum, J.T., McLeod, C.L., Shaulis, B.J., and Loocke, M. (2022) 40 years of studying Allan Hills (ALHA) 81005: What else could we possibly learn? Plenty! Lunar and Planetary Science Conference 53rd, 2756. LPI, Houston, Texas.
- Cao, H., Chen, J., Fu, X., and Ling, Z. (2020) Raman and infrared spectroscopic perspectives of lunar meteorite Northwest Africa 4884. *Journal of Raman Spectroscopy*, 51, 1652–1666, <https://doi.org/10.1002/jrs.5727>.
- Cao, H., Ling, Z., Chen, J., Fu, X., Zou, Y., and Joy, K. (2021) Petrography, mineralogy, and geochemistry of a new lunar magnesian feldspathic meteorite: Northwest Africa 11460. *Meteoritics & Planetary Science*, 56, 1857–1889, <https://doi.org/10.1111/maps.13741>.
- Corley, L.M., McGovern, P.J., Kramer, G.Y., Lemelin, M., Trang, D., Gillis-Davis, J.J., Taylor, G.J., Powell, K.E., Kiefer, W.S., Wiczorek, M., and others. (2018) Olivine-bearing lithologies on the Moon: Constraints on origins and transport mechanisms from M³ spectroscopy, radiative transfer modeling, and GRAIL crustal thickness. *Icarus*, 300, 287–304, <https://doi.org/10.1016/j.icarus.2017.09.012>.
- Dégi, J., Abart, R., Török, K., Bali, E., Wirth, R., and Rhede, D. (2010) Symplectite formation during decompression induced garnet breakdown in lower crustal mafic granulite xenoliths: Mechanisms and rates. *Contributions to Mineralogy and Petrology*, 159, 293–314, <https://doi.org/10.1007/s00410-009-0428-z>.
- Dymek, R., Albee, A., and Chodos, A. (1975) Comparative petrology of lunar cumulate rocks of possible primary origin—dunite 72415, troctolite 76535, norite 78235, and anorthosite 62237. *Lunar and Planetary Science Conference Proceedings*, 6, p. 301–341.
- Eckley, S., Zeigler, R., McCubbin, F., Needham, A., Fries, M., and Gross, J. (2020) Applicability and utility of the Astromaterials X-ray computed Tomography Laboratory at Johnson Space Center. *Lunar and Planetary Science Conference*.
- Elardo, S.M., McCubbin, F.M., and Shearer, C.K. Jr. (2012) Chromite symplectites in Mg-suite troctolite 76535 as evidence for infiltration metasomatism of a lunar layered intrusion. *Geochimica et Cosmochimica Acta*, 87, 154–177, <https://doi.org/10.1016/j.gca.2012.03.030>.
- Elkins-Tanton, L., Van Orman, J.A., Hager, B.H., and Grove, T.L. (2002a) Re-examination of the lunar magma ocean cumulate overturn hypothesis: Melting or mixing is required. *Earth and Planetary Science Letters*, 196, 239–249, [https://doi.org/10.1016/S0012-821X\(01\)00613-6](https://doi.org/10.1016/S0012-821X(01)00613-6).
- Elkins-Tanton, L.T., Van Orman, J.A., Hager, B.H., and Grove, T.L. (2002b) Re-examination of the lunar magma ocean cumulate overturn hypothesis: Melting or mixing is required. *Earth and Planetary Science Letters*, 196, 239–249, [https://doi.org/10.1016/S0012-821X\(01\)00613-6](https://doi.org/10.1016/S0012-821X(01)00613-6).
- Elkins-Tanton, L.T., Burgess, S., and Yin, Q.-Z. (2011) The lunar magma ocean: Reconciling the solidification process with lunar petrology and geochronology. *Earth and Planetary Science Letters*, 304, 326–336, <https://doi.org/10.1016/j.epsl.2011.02.004>.
- Fagan, A.L. and Gross, J. (2020) Preliminary melt models of troctolite and anorthosite clasts within Northwest Africa 11303. *Lunar and Planetary Science Conference 51st*, 51, p. 2904.pdf.
- García, R.F., Khan, A., Drilleau, M., Margerin, L., Kawamura, T., Sun, D., Wiczorek, M.A., Rivoldini, A., Nunn, C., Weber, R.C., and others. (2019) Lunar seismology: An update on interior structure models. *Space Science Reviews*, 215, 1–47, <https://doi.org/10.1007/s11214-019-0613-y>.
- Gattacceca, J., Bouvier, A., Grossman, J., Metzler, K., and Uehara, M. (2019) The Meteoritical Bulletin, No. 106. *Meteoritics & Planetary Science*, 54, 469–471, <https://doi.org/10.1111/maps.13215>.
- Goodrich, C.A., Taylor, G.J., Keil, K., Kallemeyn, G.W., and Warren, P.H. (1986) Alkali norite, troctolites, and VHK mare basalts from breccia 14304. *Journal of Geophysical Research*, 91 (B4), 305–318, <https://doi.org/10.1029/JB091iB04p0D305>.
- Gou, S., Di, K., Yue, Z., Liu, Z., He, Z., Xu, R., Lin, H., Liu, B., Peng, M., Wan, W., and others. (2019) Lunar deep materials observed by Chang'e-4 rover. *Earth and Planetary Science Letters*, 528, 115829, <https://doi.org/10.1016/j.epsl.2019.115829>.
- Gou, S., Di, K., Yue, Z., Liu, Z., He, Z., Xu, R., Liu, B., Peng, M., Wan, W., Wang, Y., and others. (2020) Forsteritic olivine and magnesium-rich orthopyroxene materials measured by Chang'e-4 rover. *Icarus*, 345, 113776, <https://doi.org/10.1016/j.icarus.2020.113776>.
- Gross, J. and Joy, K.H. (2016) Evolution, lunar: From magma ocean to crust formation. *Encyclopedia of Lunar Science*, 1–20.
- Hess, P.C. and Parmentier, E. (1995) A model for the thermal and chemical evolution of the Moon's interior: Implications for the onset of mare volcanism. *Earth and Planetary Science Letters*, 134, 501–514, [https://doi.org/10.1016/0012-821X\(95\)00138-3](https://doi.org/10.1016/0012-821X(95)00138-3).
- Hirschmann, M.M. (2000) Mantle solidus: Experimental constraints and the effects of peridotite composition. *Geochemistry, Geophysics, Geosystems*, 1, <https://doi.org/10.1029/2000GC000070>.
- Hudgins, J., Walton, E., and Spray, J. (2007) Mineralogy, petrology, and shock history of lunar meteorite Sayh al Uhaymir 300: A crystalline impact-melt breccia. *Meteoritics & Planetary Science*, 42, 1763–1779, <https://doi.org/10.1111/j.1945-5100.2007.tb00536.x>.
- Ishii, T., Miyamoto, M., and Takeda, H. (1976) Pyroxene geothermometry and crystallization-, subsolidus equilibration temperatures of lunar and achondritic pyroxenes. *Lunar and Planetary Science Conference*, 7, p. 410–412. Lunar and Planetary Institute Houston, Texas.
- Johnson, T., Morrissey, L., Nemchin, A., Gardiner, N., and Snape, J. (2021) The phases of the Moon: Modelling crystallisation of the lunar magma ocean through equilibrium thermodynamics. *Earth and Planetary Science Letters*, 556, 116721, <https://doi.org/10.1016/j.epsl.2020.116721>.
- Karato, S.-i. (2013) Geophysical constraints on the water content of the lunar mantle and its implications for the origin of the Moon. *Earth and Planetary Science Letters*, 384, 144–153, <https://doi.org/10.1016/j.epsl.2013.10.001>.
- Karner, J., Papike, J.J., and Shearer, C.K. Jr. (2003) Olivine from planetary basalts: Chemical signatures that indicate planetary parentage and those that record igneous setting and process. *American Mineralogist*, 88, 806–816, <https://doi.org/10.2138/am-2003-5-609>.
- Khan, A., Connolly, J.A., Pommier, A., and Noir, J. (2014) Geophysical evidence

- for melt in the deep lunar interior and implications for lunar evolution. *Journal of Geophysical Research. Planets*, 119, 2197–2221, <https://doi.org/10.1002/2014JE004661>.
- Kimura, M., Mikouchi, T., Suzuki, A., Miyahara, M., Ohtani, E., and Goresy, A.E. (2009) Kushiroite, $\text{CaAl}_2\text{SiO}_6$: A new mineral of the pyroxene group from the ALH 85085 CH chondrite, and its genetic significance in refractory inclusions. *American Mineralogist*, 94, 1479–1482, <https://doi.org/10.2138/am.2009.3242>.
- Klima, R.L., Pieters, C.M., Boardman, J.W., Green, R.O., Head, J.W. III, Isaacson, P.J., Mustard, J.F., Nettles, J.W., Petro, N.E., and Staid, M.I. (2011) New insights into lunar petrology: Distribution and composition of prominent low-Ca pyroxene exposures as observed by the Moon Mineralogy Mapper (M³). *Journal of Geophysical Research. Planets*, 116 (E6), <https://doi.org/10.1029/2010JE003719>.
- Korotev, R.L. (2022) Lunar meteorite: Northwest Africa 8046 clan. Washington University St. Louis, https://sites.wustl.edu/meteoritesite/items/lm_nwa_08046_clan/.
- Korotev, R.L., Zeigler, R.A., Jolliff, B.L., Irvin, A.J., and Bunch, T.E. (2009) Compositional and lithological diversity among brecciated lunar meteorites of intermediate iron concentration. *Meteoritics & Planetary Science*, 44, 1287–1322, <https://doi.org/10.1111/j.1945-5100.2009.tb01223.x>.
- Kramer, G.Y., Kring, D.A., Nahm, A.L., and Pieters, C.M. (2013) Spectral and photogeologic mapping of Schrödinger Basin and implications for post-South Pole-Aitken impact deep subsurface stratigraphy. *Icarus*, 223, 131–148, <https://doi.org/10.1016/j.icarus.2012.11.008>.
- Kurat, G. and Brandstätter, F. (1983) Meteorite ALHA81005: Petrology of a new lunar highland sample. *Geophysical Research Letters*, 10, 795–798, <https://doi.org/10.1029/GL010i009p00795>.
- Kuskov, O. and Kronrod, V. (2009) Geochemical constraints on the model of the composition and thermal conditions of the Moon according to seismic data. *Izvestiya Physics of the Solid Earth*, 45, 753–768, <https://doi.org/10.1134/S1069351309090043>.
- Landgrebe, D. and Biehl, L. (2011) An Introduction and Reference for Multispec©, 193 p. Purdue University. https://engineering.purdue.edu/~biehl/MultiSpec/MultiSpec_Intro_9_11.pdf.
- Lemelin, M., Lucey, P.G., Miljković, K., Gaddis, L.R., Hare, T., and Ohtake, M. (2019) The compositions of the lunar crust and upper mantle: Spectral analysis of the inner rings of lunar impact basins. *Planetary and Space Science*, 165, 230–243, <https://doi.org/10.1016/j.pss.2018.10.003>.
- Li, C., Liu, D., Liu, B., Ren, X., Liu, J., He, Z., Zuo, W., Zeng, X., Xu, R., Tan, X., and others. (2019) Chang'E-4 initial spectroscopic identification of lunar farside mantle-derived materials. *Nature*, 569, 378–382, <https://doi.org/10.1038/s41586-019-1189-0>.
- Lin, Y., Hui, H., Xia, X., Shang, S., and van Westrenen, W. (2020) Experimental constraints on the solidification of a hydrous lunar magma ocean. *Meteoritics & Planetary Science*, 55, 207–230, <https://doi.org/10.1111/maps.13425>.
- Lindsley, D.H. (1983) Pyroxene thermometry. *American Mineralogist*, 68, 477–493.
- Lindstrom, M.M., Knapp, S.A., Shervais, J.W., and Taylor, L.A. (1984) Magnesian anorthosites and associated troctolites and dunite in Apollo 14 breccias. *Journal of Geophysical Research*, 89 (S01), C41–C49, <https://doi.org/10.1029/JB089iS01p00C41>.
- Longhi, J. (2006) Petrogenesis of picritic mare magmas: Constraints on the extent of early lunar differentiation. *Geochimica et Cosmochimica Acta*, 70, 5919–5934, <https://doi.org/10.1016/j.gca.2006.09.023>.
- Lunning, N.G. and Gross, J. (2019) Lunar feldspathic regolith breccia with magnesium-rich components: Northwest Africa 11303. *Lunar and Planetary Science Conference 50th*, 50, 2407. LPI, Houston, Texas.
- Maloy, A.K. and Treiman, A.H. (2007) Evaluation of image classification routines for determining modal mineralogy of rocks from X-ray maps. *American Mineralogist*, 92, 1781–1788, <https://doi.org/10.2138/am.2007.2477>.
- Marvin, U., Holmberg, B., and Lindstrom, M. (1989a) Granoblastic lunar “dunites” revisited. 52nd Annual Meeting of the Meteorological Society, p. 148.
- (1989b) Polygonized lunar “dunites” revisited. *Meteoritics & Planetary Science*, 24, 299.
- (1991) New observations on polygonized lunar dunites. *Lunar and Planetary Science Conference 22nd*, 22, p. 859–860.
- Matsumoto, K., Yamada, R., Kikuchi, F., Kamata, S., Ishihara, Y., Iwata, T., Hanada, H., and Sasaki, S. (2015) Internal structure of the Moon inferred from Apollo seismic data and selenodetic data from GRAIL and LLR. *Geophysical Research Letters*, 42, 7351–7358, <https://doi.org/10.1002/2015GL065335>.
- Matsuyama, I., Nimmo, F., Keane, J.T., Chan, N.H., Taylor, G.J., Wieczorek, M.A., Kiefer, W.S., and Williams, J.G. (2016) GRAIL, LLR, and LOLA constraints on the interior structure of the Moon. *Geophysical Research Letters*, 43, 8365–8375, <https://doi.org/10.1002/2016GL069952>.
- McCallum, I.S. and Schwartz, J.M. (2001) Lunar Mg suite: Thermobarometry and petrogenesis of parental magmas. *Journal of Geophysical Research*, 106 (E11), 27969–27983, <https://doi.org/10.1029/2000JE001397>.
- Mercur, C.N., Treiman, A.H., and Joy, K.H. (2013) New lunar meteorite Northwest Africa 2996: A window into farside lithologies and petrogenesis. *Meteoritics & Planetary Science*, 48, 289–315, <https://doi.org/10.1111/maps.12056>.
- Mercier, J.C. and Nicolas, A. (1975) Textures and fabrics of upper-mantle peridotites as illustrated by xenoliths from basalts. *Journal of Petrology*, 16, 454–487, <https://doi.org/10.1093/petrology/16.1.454>.
- Meyer, C. Jr. (2012) Lunar Sample Compendium 2022. Johnson Space Center, NASA, <https://curator.jsc.nasa.gov/lunar/lsc/index.cfm>.
- Miljković, K., Wieczorek, M.A., Collins, G.S., Solomon, S.C., Smith, D.E., and Zuber, M.T. (2015) Excavation of the lunar mantle by basin-forming impact events on the Moon. *Earth and Planetary Science Letters*, 409, 243–251, <https://doi.org/10.1016/j.epsl.2014.10.041>.
- Moriarty, D., Pieters, C., and Isaacson, P. (2013) Compositional heterogeneity of central peaks within the South Pole-Aitken Basin. *Journal of Geophysical Research. Planets*, 118, 2310–2322, <https://doi.org/10.1002/2013JE004376>.
- Moriarty, D.P. III, Dygert, N., Valencia, S.N., Watkins, R.N., and Petro, N.E. (2021a) The search for lunar mantle rocks exposed on the surface of the Moon. *Nature Communications*, 12, 4659, <https://doi.org/10.1038/s41467-021-24626-3>.
- Moriarty, D. III, Watkins, R., Valencia, S., Kendall, J., Evans, A., Dygert, N., and Petro, N. (2021b) Evidence for a stratified upper mantle preserved within the South Pole-Aitken Basin. *Journal of Geophysical Research: Planets*, 126(1), e2020JE006589.
- Morris, R., Taylor, G., Newsom, H., Keil, K., and Garcia, S. (1990) Highly evolved and ultramafic lithologies from Apollo 14 soils. *Lunar and Planetary Science Conference Proceedings*, 20, p. 61–75.
- Morrison, D.A. (1998) Did a thick South Pole-Aitken Basin melt sheet differentiate to form cumulates? *Lunar and Planetary Science Conference*.
- Nakamura, R., Matsunaga, T., Ogawa, Y., Yamamoto, S., Hiroi, T., Saiki, K., Hirata, N., Arai, T., Kitazato, K., Takeda, H., and others. (2009) Ultramafic impact melt sheet beneath the South Pole–Aitken basin on the Moon. *Geophysical Research Letters*, 36, L22202, <https://doi.org/10.1029/2009GL040765>.
- Nazarov, M.A., Demidova, S.I., Patchen, A., and Taylor, L.A. (2004) Dhofar 311, 730 and 731: New lunar meteorites from Oman. *Lunar and Planetary Science*, 2181V, 1233.
- Nelson, W.S., Hammer, J.E., Shea, T., Hellebrand, E., and Jeffrey Taylor, G. (2021) Chemical heterogeneities reveal early rapid cooling of Apollo Troctolite 76535. *Nature Communications*, 12, 7054, <https://doi.org/10.1038/s41467-021-26841-4>.
- Potter, R., Kring, D., Collins, G., Kiefer, W., and McGovern, P. (2012) Estimating transient crater size using the crustal annular bulge: Insights from numerical modeling of lunar basin-scale impacts. *Geophysical Research Letters*, 39, <https://doi.org/10.1029/2012GL052981>.
- Powell, R. and Holland, T. (1994) Optimal geothermometry and geobarometry. *American Mineralogist*, 79, 120–133.
- Powell, R. and Holland, T.J.B. (2008) On thermobarometry. *Journal of Metamorphic Geology*, 26, 155–179, <https://doi.org/10.1111/j.1525-1314.2007.00756.x>.
- Putirka, K.D. (2008) Thermometers and barometers for volcanic systems. *Reviews in Mineralogy and Geochemistry*, 69, 61–120, <https://doi.org/10.2138/rmg.2008.69.3>.
- Rapp, J. and Draper, D. (2018) Fractional crystallization of the lunar magma ocean: Updating the dominant paradigm. *Meteoritics & Planetary Science*, 53, 1432–1455, <https://doi.org/10.1111/maps.13086>.
- Saini, R., Mijajlovic, T., Herd, C.D.K., and Walton, L.A. (2022) Northwest Africa 14340: Petrological characterization and shock metamorphism of a lunar regolith breccia. 85th Annual Meeting of The Meteoritical Society, Glasgow, Scotland.
- Schmitt, H. (2016) Symplectites in Dunite 72415 and Troctolite 76535 Indicate Mantle Overtun Beneath Lunar Near-Side. 47th Annual Lunar and Planetary Science Conference, p. 2339.
- Schwinger, S. and Breuer, D. (2022) Employing magma ocean crystallization models to constrain structure and composition of the lunar interior. *Physics of the Earth and Planetary Interiors*, 322, 106831, <https://doi.org/10.1016/j.pepi.2021.106831>.
- Shearer, C.K. and Papike, J. (1999) Magmatic evolution of the Moon. *American Mineralogist*, 84, 1469–1494, <https://doi.org/10.2138/am-1999-1001>.
- Shearer, C.K., Burger, P.V., Bell, A.S., Guan, Y., and Neal, C.R. (2015a) Exploring the Moon’s surface for remnants of the lunar mantle 1. Dunite xenoliths in mare basalts. A crustal or mantle origin? *Meteoritics & Planetary Science*, 50, 1449–1467, <https://doi.org/10.1111/maps.12480>.
- Shearer, C.K., Elardo, S.M., Petro, N.E., Borg, L.E., and McCubbin, F.M. (2015b) Origin of the lunar highlands Mg-suite: An integrated petrology, geochemistry, chronology, and remote sensing perspective. *American Mineralogist*, 100, 294–325, <https://doi.org/10.2138/am-2015-4817>.
- Sheikh, D., Ruzicka, A., Hutson, M.L., and Stream, M. (2022) Dunite clast in lunar meteorites Northwest Africa (NWA) 14900: Mantle Derived? *Meteoritics & Planetary Science*, 57 (S1), 433.
- Shervais, J.W. and McGee, J.J. (1999) Petrology of the Western Highland Province: Ancient crust formation at the Apollo 14 site. *Journal of Geophysical Research*, 104 (E3), 5891–5920, <https://doi.org/10.1029/1998JE00025>.
- Shervais, J.W., Taylor, L.A., Laul, J., and Smith, M. (1984) Pristine highland clasts in consortium breccia 14305: Petrology and geochemistry. *Journal of Geophysical Research*, 89 (S01), C25–C40, <https://doi.org/10.1029/JB089iS01p00C25>.

- Snyder, G.A., Taylor, L.A., and Neal, C.R. (1992) A chemical model for generating the sources of mare basalts: Combined equilibrium and fractional crystallization of the lunar magmasphere. *Geochimica et Cosmochimica Acta*, 56, 3809–3823, [https://doi.org/10.1016/0016-7037\(92\)90172-F](https://doi.org/10.1016/0016-7037(92)90172-F).
- Snyder, G.A., Taylor, L.A., and Halliday, A.N. (1995) Chronology and petrogenesis of the lunar highlands alkali suite: Cumulates from KREEP basalt crystallization. *Geochimica et Cosmochimica Acta*, 59, 1185–1203, [https://doi.org/10.1016/0016-7037\(95\)00034-W](https://doi.org/10.1016/0016-7037(95)00034-W).
- Spry, A. (1969) *Metamorphic Textures*. Pergamon Press.
- Srivastava, Y., Basu Sarbadhikari, A., Day, J.M.D., Yamaguchi, A., and Takenouchi, A. (2022) A changing thermal regime revealed from shallow to deep basalt source melting in the Moon. *Nature Communications*, 13, 7594, <https://doi.org/10.1038/s41467-022-35260-y>. PubMed
- Sugihara, T., Ohtake, M., Owada, A., Ishii, T., Otsuki, M., and Takeda, H. (2004) Petrology and reflectance spectroscopy of lunar meteorite Yamato 981031: Implications for the source region of the meteorite and remote-sensing spectroscopy. *Antarctic Meteorite Research*, 17, 209.
- Taylor, G.J. and Marvin, U.B. (1971) A dunite-norite lunar microbreccia. *Meteoritics*, 6, 173.
- Treiman, A.H. and Coleff, D.M. (2018) Lunar meteorite Northwest Africa (NWA) 11421: X-ray tomography and preliminary petrology. *Meteoritics and Planetary Science*, 53, Abstract 6329.
- Treiman, A.H. and Semprich, J. (2019) Dunite in lunar meteorite Northwest Africa 11421: Petrology and origin. *Lunar and Planetary Science Conference 50th*, 50 p. Abstract 1225. Lunar and Planetary Institute.
- (2021) Lunar feldspathic breccia Northwest Africa (NWA) 11421: Clasts in the corners. *Lunar and Planetary Science Conference 52nd*, 6065. Lunar and Planetary Institute, Houston, Texas.
- Vaci, Z., Day, J., Paquet, M., Ziegler, K., Yin, Q.-Z., Dey, S., Miller, A., Agee, C., Bartoschewitz, R., and Pack, A. (2021) Olivine-rich achondrites from Vesta and the missing mantle problem. *Nature Communications*, 12, 1–8.
- Vaughan, W.M., Head, J.W., Wilson, L., and Hess, P.C. (2013) Geology and petrology of enormous volumes of impact melt on the Moon: A case study of the Orientale basin impact melt sea. *Icarus*, 223, 749–765, <https://doi.org/10.1016/j.icarus.2013.01.017>.
- Wager, L.R. and Brown, G.M. (1967) Layered Igneous Rocks, 588 p. WH Freeman.
- Wager, L., Brown, G., and Wadsworth, W. (1960) Types of igneous cumulates. *Journal of Petrology*, 1, 73–85, <https://doi.org/10.1093/ptrology/1.1.73>.
- Warren, P.H., Taylor, G.J., and Keil, K. (1983) Regolith breccia Allan Hills A81005: Evidence of lunar origin, and petrography of pristine and nonpristine clasts. *Geophysical Research Letters*, 10, 779–782, <https://doi.org/10.1029/GL010i009p00779>.
- Warren, P.H., Jerde, E.A., and Kallemeyn, G.W. (1987) Pristine Moon rocks: A “large” felsite and a metal-rich ferroan anorthosite. *Journal of Geophysical Research*, 92 (B4), E303–E313, <https://doi.org/10.1029/JB092iB04p0E303>.
- Wieczorek, M.A., Jolliff, B.L., Khan, A., Pritchard, M.E., Weiss, B.P., Williams, J.G., Hood, L.L., Richter, K., Neal, C.R., and Shearer, C.K. (2006) The constitution and structure of the lunar interior. *Reviews in Mineralogy and Geochemistry*, 60, 221–364, <https://doi.org/10.2138/rmg.2006.60.3>.
- Wieczorek, M.A., Neumann, G.A., Nimmo, F., Kiefer, W.S., Taylor, G.J., Melosh, H.J., Phillips, R.J., Solomon, S.C., Andrews-Hanna, J.C., Asmar, S.W., and others. (2013) The crust of the Moon as seen by GRAIL. *Science*, 339, 671–675, <https://doi.org/10.1126/science.1231530>.
- Wood, J.A., Dickey, J.S. Jr., Marvin, U.B., and Powell, B.N. (1970) Lunar anorthosites. *Science*, 167, 602–604, <https://doi.org/10.1126/science.167.3918.602>.
- Yamamoto, S., Nakamura, R., Matsunaga, T., Ogawa, Y., Ishihara, Y., Morota, T., Hirata, N., Ohtake, M., Hiroi, T., Yokota, Y., and others. (2010) Possible mantle origin of olivine around lunar impact basins detected by SELENE. *Nature Geoscience*, 3, 533–536, <https://doi.org/10.1038/ngeo897>.
- Zeigler, R.A., Coleff, D., and McCubbin, F.M. (2017) The Astromaterials X-ray Computed Tomography Laboratory at Johnson Space Center. *Lunar and Planetary Science Conference*.
- Zeng, X., Li, S., Joy, K.H., Li, X., Liu, J., Li, Y., Li, R., and Wang, S. (2020) Occurrence and implications of secondary olivine veinlets in lunar highland breccia Northwest Africa 11273. *Meteoritics & Planetary Science*, 55, 36–55, <https://doi.org/10.1111/maps.13421>.
- Zhao, D., Arai, T., Liu, L., and Ohtani, E. (2012) Seismic tomography and geochemical evidence for lunar mantle heterogeneity: Comparing with Earth. *Global and Planetary Change*, 90–91, 29–36, <https://doi.org/10.1016/j.gloplacha.2012.01.004>.
- Zhao, Y., De Vries, J., van den Berg, A., Jacobs, M., and van Westrenen, W. (2019) The participation of ilmenite-bearing cumulates in lunar mantle overturn. *Earth and Planetary Science Letters*, 511, 1–11, <https://doi.org/10.1016/j.epsl.2019.01.022>.

MANUSCRIPT RECEIVED DECEMBER 14, 2022

MANUSCRIPT ACCEPTED MAY 3, 2023

ACCEPTED MANUSCRIPT ONLINE MAY 18, 2023

MANUSCRIPT HANDLED BY HEATHER WATSON

Endnote:

¹Deposit item AM-23-128911. Online Materials are free to all readers. Go online, via the table of contents or article view, and find the tab or link for supplemental materials.